Optimization and evaluation of a semi-submersible wind turbine and oscillating body wave energy converters hybrid system

Jin, Peng
School of Civil Engineering and Transportation, South China University of Technology

Zheng, Zhi
School of Civil Engineering and Transportation, South China University of Technology

Zhou, Zhaomin
PowerChina Renewable Energy Co., LTD.

Zhou, Binzhen
Donghai Laboratory

他

出版情報：Energy. 282, pp.128889-, 2023-11-01. Elsevier
バージョン：
権利関係：

Optimization and evaluation of a semi-submersible wind turbine and oscillating body wave energy converters hybrid system

Peng Jin[b,c], Zhi Zheng[b], Zhaomin Zhou[d], Binzhen Zhou[a,b,*], Lei Wang[b], Yang Yang[e], Yingyi Liu[f]

[a] *Donghai Laboratory, Zhoushan Zhejiang 316021, China*

[b] *School of Civil Engineering and Transportation, South China University of Technology, Guangzhou 510641, China*

[c] *State Key Laboratory of Coastal and Offshore Engineering, Dalian University of Technology, Dalian, 116024, China*

[d] *PowerChina renewable energy Co., LTD., Beijing 100101, China*

[e] *Faculty of Maritime and Transportation, Ningbo University, Ningbo, 315211, China*

[f] *Research Institute for Applied Mechanics, Kyushu University, Kasuga, 816-8580, Japan*

Abstract

A hybrid system consisting of a floating offshore wind turbine and wave energy converters (WECs) is promising for multiple extractions of ocean renewable energy. Optimization of the layout and an evaluation of the performance of the hybrid systems are important before practical use but are not well done due to limited simulation tools. This study fills these gaps by proposing a complete toolkit based on the OpenFAST-AQWA framework together with a code that can deal with the full couplings in the problem. A novel DeepCWind-Wave Stars hybrid system is proposed as a representative to validate and practice the new tool. The key parameters of the WECs are optimized using an easily performed method based on the local wave contour disturbed by the platform. Motions, mooring loads, and power of the hybrid system are evaluated under a wide range of wind and wave conditions to examine the influence of the WECs. Results show that the integration of the WECs brings no harm to the stability of the system. The WECs reduce the fluctuation in the mooring force but slightly increase the average mooring force. The generated wave power is an adequate supplement to wind power, especially at a small wind speed.

Keywords: wind energy, wave energy, hybrid system, semi-submersible wind platform, Wave Star

1. Introduction

Ocean renewable energy has been thriving and extensively developed in recent years based on a worldwide consensus about a low-carbon economy [1]-[3]. To fully use the abundant renewable energy resources in the ocean, co-located energy extraction by combining different kinds of ocean renewable energy equipment becomes a research frontier [4]-[6]. Hybrid systems consisting of offshore wind turbines [7] and wave energy converters (WECs) [8]-[10] provide a promising scenario of sufficient use of the strong sea wind and high waves, offering an excellent synergetic application since the high winds and waves often coexist [11]. Such combinations also show several merits of mutual benefits in addition to more sufficient use of the local energy resource [12]. For example, wave energy is less developed than offshore wind energy and is still an industry in its early age, facing the problem of high cost [13].

* Corresponding authors
E-mail address: zhoubinzhen@scut.edu.cn (B. Zhou)

By integrating WECs on an offshore wind turbine, the turbine can share infrastructure such as moorings, supporting structures, power grids, and maintenance with the WECs, helping reduce the cost of the WECs [14]-[16]. In turn, the power generated by the WECs can compensate for the shortage of power output of the wind turbine during its downtime, improving the stability of power generation [17][18]. Till now, many concepts of wind-wave hybrid systems have been proposed (for example, in refs [19]-[23]) inspired by government or industrial support through innovative projects such as the EU EP7 MARINA [24].

Although many concepts of wind-wave hybrid systems have been proposed and extensively studied, none have been constructed and applied in the real world. Few of them are in the sea trail stage. The speed of development of hybrid systems depends on the technological maturity of wind and wave energy equipment and their compatibility. Nowadays, the technology of rotor and nacelle is quite mature owing to the long development of onshore wind turbines [25][26]. The turbine's capacity can be above 10 MW in the current industry standard [27]. The support structure of offshore wind turbines is still under fast development. Although the technology of fixed foundations [28][29] is more mature than floating foundations, fixed foundations can hardly support a turbine larger than 2 MW due to their structural strength [30]. Floating foundations can support much larger turbines and work in deep seas, where the wind and wave resources are more abundant, proving it is a future development trend for offshore wind turbines. Among the three prevailing types of floating foundations (Spar, tension leg platform, and semi-submersible platform), the semi-submersible type accounts for most of the existing platforms [28]. Turning to the WECs, wave energy is a much younger industry with rapid development in recent years compared with offshore wind. Many WECs based on different energy extraction mechanisms have been proposed, but few reach a commercial application level. Nielsen *et al*. [31] evaluated the Technology Readiness Level (TRL) of prevailing WECs concerning the Danish Projects and showed that the technology of Wave Star [32] has the highest TRL (TRL 7). Besides, as an oscillating body WEC, Wave Star is easily deployed and installed on an existing floating wind turbine. Based on the above evidence, a wind-wave hybrid system in the form of the semi-submersible platform and Wave Star combination is quite promising and ready for practical co-located ocean renewable energy extractions. Several concepts of such combination have been proposed, such as in refs. [33]-[36].

Before construction and commercial application, a proper design based on a thorough evaluation of the hybrid system in a wide range of wind and wave conditions are necessary. This relies on an accurate and reliable numerical model. As interdisciplinary equipment, the hybrid system can hardly be well treated by traditional software or code of only wind turbines or hydrodynamics. A combined toolkit is widely applied since, till now, there is not a complete tool for a hybrid system. The integrated toolkit commonly includes an aero-servo part, a hydro part, and a tool that can bridge the two by conveying information about motions and forces. Hu *et al*. [14] used a combination of WAFDUT and the empirical

formula of wind force and torque. Muliawan *et al*. [37] used a SIMO-TDHMILL3D combination. Yde *et al*. [38] used a HAWC2-WAMSIM combination. Ren *et al*. [22] and Si *et al*. [35] used AQWA to simulate the hydrodynamics of their wind-wave hybrid systems. The wind loads were simplified as a sum of thrust force and torque through the empirical formula and implemented by the user-force function module in AQWA. Karimirad and Koushan [39], Michailides *et al*. [23], Gao *et al*. [40], and Luan *et al*. [41] applied a combined toolkit of SIMO-RIFLEX-AeroDyn. Their time-domain model employed a flexible joint to simulate the relative rotation between the main shaft and the tower. It implemented the one-way delivery of the loads on the rotor and nacelle to the tower.

Although the development of semi-submersible platforms and Wave Stars hybrid systems are thriving, two critical gaps remain. First, in previous studies, Wave Stars are directly attached to a floating platform without optimization of their layout. Optimization of a WEC is essential to the power output. The difference between an optimized WEC and an unoptimized WEC and between a well-designed layout and an ill-designed layout can be huge. An optimization would be mandatory in the early design stage. Second, till now, the existing simulation toolkits cannot effectively deal with the couplings between different parts in the system and the wave-structure interaction. For example, the SIMO-RIFLEX-AeroDyn combination fails to consider the delivery of the motion of the floating bodies to the servo of the turbine; the AQWA and user-force function combination assumes constant wind force and torque. The widely used FAST is powerful in simulating wind turbines but cannot simulate multi-body dynamics. While only part of the couplings between different subsystems is considered, it leaves uncertainty and inaccuracy in the design and evaluation of the system. Therefore, a complete toolkit is required. This study aims to fill these gaps. A complete toolkit combining FAST and AQWA and an F2A [42] (FAST to AQWA) code in the form of DLL that can convey full coupling information between the two is proposed, which is similar to those employed in Zhang *et al*. [43] and Chen *et al*. [44]. A new DeepCWind-Wave Stars hybrid system is proposed, and the key parameters of the layout of the Wave Stars are optimized using a novel, straightforward method based on the local wave contour shaped by the radiation and diffraction of the platform. A relatively thorough evaluation of the optimized hybrid system is also performed under a wide range of wind and wave conditions. These techniques can be readily used in other wind-wave hybrid systems.

The rest of the paper is organized as follows. In Section 2, the configurations of the DeepCWind semi-submersible floating offshore wind turbine, the Wave Star, and the hybrid system are described, providing their key parameters. In Section 3, the fundamental theory behind the F2A code is interpreted and validated. In Section 4, the key parameters of the layout of the Wave Stars are optimized. And an analysis of the influence of the Wave Stars on the motions, mooring loads, and power performance of the wind turbine and the hybrid system is performed. In Section 5, the major conclusion is drawn.

2. DeepCWind-Wave Stars hybrid system

In this section, the configuration of the present DeepCWind-Wave Stars hybrid system is illustrated. Key parameters of DeepCWind and Wave Star are also given.

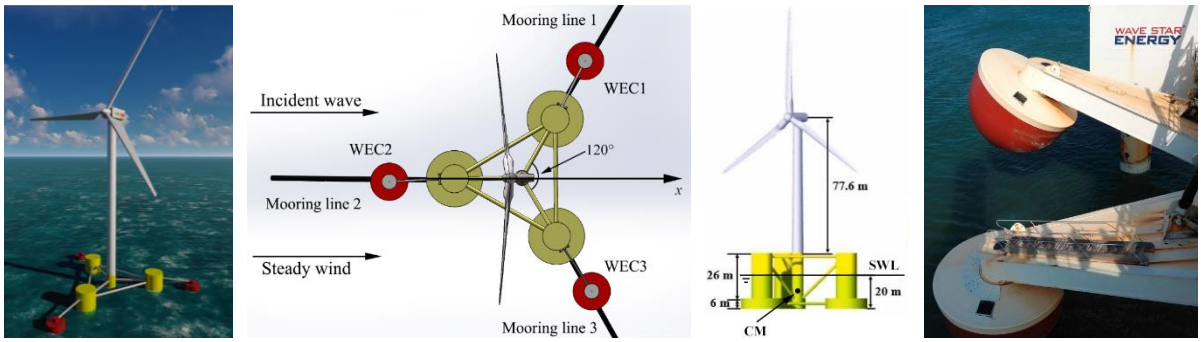

(a) Hybrid system (b) Configuration of hybrid system (c) DeepCWind (d) Wave Star [45]

Figure 1 Sketch and configuration of the DeepCWind-Wave Stars hybrid system and its components

2.1 DeepCWind

The semi-submersible floating offshore wind turbine DeepCWind [46] (Figure 1c) is developed by National Renewable Energy Laboratory (NREL) [47]. The platform comprises a central and three side columns equipped with heave plates [48]. The draft of the platform is 20 m. A 5MW wind turbine is installed on the tower standing on the central column. The tower base is 10 m above the mean water level. Generator torque control and blade pitch regulation are applied on the NREL 5 MW wind turbine for maximum power tracking and power regulation below and above the rated conditions. A three-cable catenary mooring system is used to prevent the hybrid system from drifting away under the action of wind and wave loads. Key parameters of the subsystems of the platform, wind turbine, and mooring of DeepCWind are shown in Table 1.

Table 1 Key parameters of DeepCwind [47]

Subsystem	Item	Value and unit
Platform	Draft	20 m
	Elevation of center column (tower base) above SWL	10 m
	Elevation of offset columns above SWL	12 m
	Spacing between offset columns	50 m
	Length of upper columns	26 m
	Length of base columns	6 m
	Depth to top of base columns below SWL	14 m
	Diameter of central column	6.5 m
	Diameter of offset (upper) columns	12 m
	Diameter of offset (upper) columns	24 m
	Diameter of pontoons and cross braces	1.6 m
	Platform mass, including ballast	1.35×10^7 kg

	CM location below SWL	13.46 m
	Platform roll inertia about CM	6.827×10^{9} kg·m^2
	Platform pitch inertia about CM	6.827×10^{9} kg·m^2
	Platform yaw inertia about CM	1.226×10^{10} kg·m^2
Wind turbine (NREL 5 MW)	Rotor diameter	126 m
	Hub diameter	3 m
	Hub height	90 m
	Shaft tilt	5 deg
	Rotor mass	1.1×10^{5} kg
	Nacelle mass	2.4×10^{5} kg
	Tower mass	3.47×10^{5} kg
Mooring	Number of mooring lines	3
	Angle between adjacent lines	120 deg
	Depth to anchors below SWL	200 m
	Depth to fairleads below SWL	14 m
	Radius to anchors from platform centerline	40.868 m
	Unstretched mooring line length	835.5 m
	Mooring line diameter	0.0766 m
	Equivalent mooring line mass density	113.35 kg/m
	Equivalent mooring line mass density in water	108.35 kg/m
	Equivalent mooring line extensional stiffness [59][60]	753.6 MN
	Hydrodynamic drag coefficient for mooring lines	1.1
	Hydrodynamic added-mass coefficient for mooring lines	1.0
	Seabed drag coefficient for mooring lines	1.0
	Structural damping of mooring lines	0.02

2.2 Wave Star

Wave Star (Figure 1d) is regarded as one of the most successful point-absorber WEC models with a relatively high TRL. The main part is a semispherical buoy hanging by an arm. The buoy containing a ballast tank is made of glass fibre. The ballast tank is filled with water to reduce its natural frequency for better power generation in long waves. A hydraulic cylinder is attached to the buoy that can help lift the buoy out of the water while encountering extreme environmental conditions to protect it from destruction. In operational conditions, the buoy is forced up and down by the waves, and the reciprocating heave motion of the buoy drives the rotation of the arm. The root of the arm is hinged to a support structure through a shaft where the power take-off (PTO) system is embedded. The rotation of the arm drives the PTO system to generate electric power. The arm rotation drives the hydraulic PTO for wave power generation.

In this study, the complex truss arm of Wave Star is simplified and idealized as a massless rod (Figure 2). The length of the arm and the height of the hinge point can be defined by the flowing equation:

$$L_{\mathrm{h}} = L\sin\varphi \tag{1}$$

where L and L_h are the arm length and its horizontal projection, respectively. φ is the angle contained by the arm and the vertical axis. The hybrid system is planned to be deployed in an operational site in the South China Sea. The peak wave period there is T_p = 5.3 s [14]. The arm projection and contained angle of the Wave Stars are to be optimized according to this wave state, while the buoy with the existing mature design is used. Key parameters of the optimized Wave Star buoy are shown in Table 2.

Table 2 Key parameters of Wave Star

Item	Value
Diameter at the SWL	9.8 m
Draft	4 m
Elevation of WECs above SWL	3.2 m
Mass	188727 kg
CM location below SWL	1.4545 m
Roll inertia about CM	1029 000 kg·m^2
Pitch inertia about CM	1029 000 kg·m^2
Yaw inertia about CM	1704 000 kg·m^2

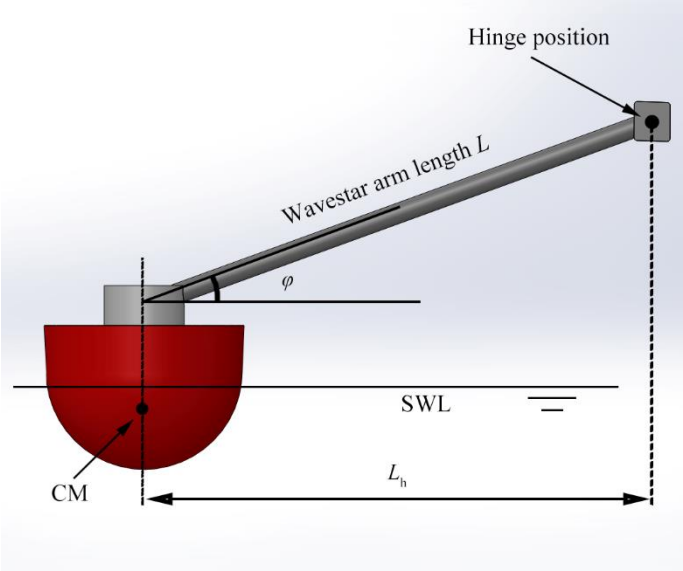

Figure 2 Sketch of the present Wave Star

2.3 Hybrid system

The 3D rendered scheme of the DeepCWind-Wave Stars hybrid system is shown in Figure 1a, and its layout is shown in Figure 1b. Three Wave Stars are respectively installed on each side column of the platform. They are named WEC #1, WEC #2, and WEC #3, respectively. Like the side columns of the platform, each pair of Wave Stars contains an angle of 120°.

3. Mathematical model

The DeepCWind-Wave Stars hybrid system is simulated in a FAST-to-AQWA framework. The FAST and AQWA are mature open-source and commercial software, respectively. Their fundamental

aerodynamic and hydrodynamic theories can be easily referred to in the user manuals [49][50] and will not be introduced here. The F2A DLL file is a code based on the work of Yang *et al*. [42] to connect FAST and AQWA and convey information on motions and forces between the two. The fundamental theory that forms the basis of the F2A code and how it works to bridge FAST and AQWA are described in this section.

3.1 Motion equation

Based on Cummins' equation [51], the matrix form multi-body motion equation of the DeepCWind-Wave Stars hybrid system is

$$\left[\mathbf{M}+\mathbf{A}_{\infty}\right]\ddot{\mathbf{X}}(t)+\mathbf{K}\mathbf{X}(t)+\int_{0}^{t}\mathbf{R}(t-\tau)\dot{\mathbf{X}}(\tau)d\tau=\mathbf{F}_{\mathrm{ex}}(t)+\mathbf{F}_{\mathrm{c}}(t) \tag{2}$$

where $\mathbf{X}(t)$, $\dot{\mathbf{X}}(t)$, and $\ddot{\mathbf{X}}(t)$ are the vectors of displacement, velocity, and acceleration, respectively. $\mathbf{M}$ is the matrix of mass. $\mathbf{A}_{\infty}$ is the matrix of added mass at infinite wave frequency, which can be calculated using a refined Filon quadrature method proposed by Liu [52]. The added mass, radiation damping, and wave excitation force are all calculated in AQWA based on the potential flow theory of linear waves. $\mathbf{K}$ is the matrix of the hydrostatic restoration coefficient. $\mathbf{R}$ is the matrix of radiation impulse response function (RIRF). t and τ are time terms. $\mathbf{F}_{\mathrm{c}}(t)$ is the constraint force, which can be dealt with using the augment method based on the Lagrange multiplier [53]. $\mathbf{F}_{\mathrm{ex}}(t)$ is the sum of external forces:

$$\mathbf{F}_{\mathrm{ex}}\left(t\right)=\mathbf{F}_{\mathrm{wave}}\left(t\right)+\mathbf{F}_{\mathrm{PTO}}\left(t\right)+\mathbf{F}_{\mathrm{wind}}\left(\mathbf{X},t\right)+\mathbf{F}_{\mathrm{moor}}\left(\mathbf{X},t\right)+\mathbf{F}_{\mathrm{vis}}\left(t\right) \tag{3}$$

where $\mathbf{F}_{\mathrm{wave}}(t)$, $\mathbf{F}_{\mathrm{PTO}}(t)$, $\mathbf{F}_{\mathrm{wind}}(t)$, $\mathbf{F}_{\mathrm{moor}}(t)$, and $\mathbf{F}_{\mathrm{vis}}(t)$ are the wave excitation force, power take-off force, aerodynamic force, mooring force, and fluid viscous force, respectively. The viscous correction for the DeepCWind platform is calculated by the method of critical damping [54]. The viscous damping (1.17×10^{6} N·s/m in the surge direction, 1.15×10^{6} N·s/m in the heave direction, and 6.14×10^{8} N·m·s/rad in the pitch direction) is taken as 8% of the critical damping in each direction. For the Wave Star, Zhou *et al*. [55] performed a rigorous investigation and showed that viscosity can be almost neglected for a hemispherical buoy like the present one. Therefore, the viscous correction of the Wave Star is neglected in the present research.

3.2 Power take-off

Linear power take-off damping b_{PTO} is assumed. The power take-off force on the hinge and the wave power generated by a Wave Star are:

$$F_{\mathrm{PTO}}=b_{\mathrm{PTO}}\dot{\theta}(t) \tag{4}$$

$$P=F_{\mathrm{PTO}}\dot{\theta}(t)=b_{\mathrm{PTO}}\dot{\theta}^{2}(t) \tag{5}$$

where θ and $\dot{\theta}$ are the angular displacement and velocity relative to the hinge, respectively, with

$$\theta = \arccos \sqrt{\frac{(L^2_{JW} + L^2_{JP} - L^2_{WP})}{2 \times L_{JW} \times L_{JP}}} \tag{6}$$

where L_{JW}, L_{JP} and L_{WP} are the characteristic lengths illustrated in Figure 3.

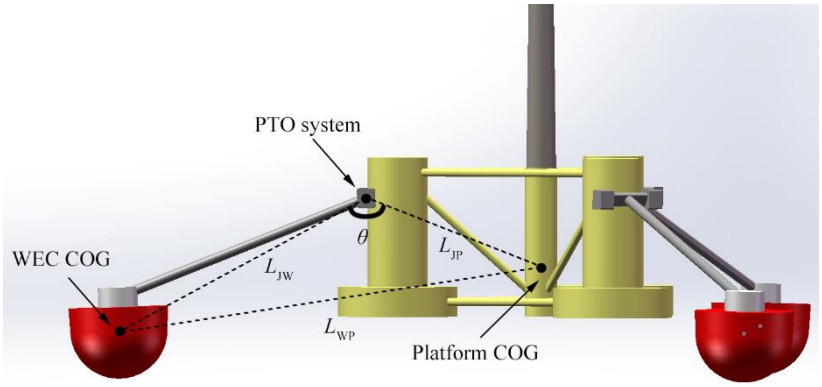

Figure 3 Profile of the Wave Stars in the hybrid system

3.3 Coupling framework of F2A

The full coupling in the FAST-to-AQWA framework is illustrated in Figure 4. The aerodynamic loads on the blades, nacelle, and tower are calculated according to the wind speed and position of the turbine and are delivered by F2A to the platform. The displacement and velocity of the platform are, in turn, delivered by F2A to the wind turbine. The hydrodynamic couplings between the platform and the Wave Stars are included in AQWA. The constraints and PTOs between the platform and the Wave Stars are considered in the motion equation (Eq. (2)). The mooring loads are calculated in AQWA according to the position of the platform and, in turn, delivered to the platform.

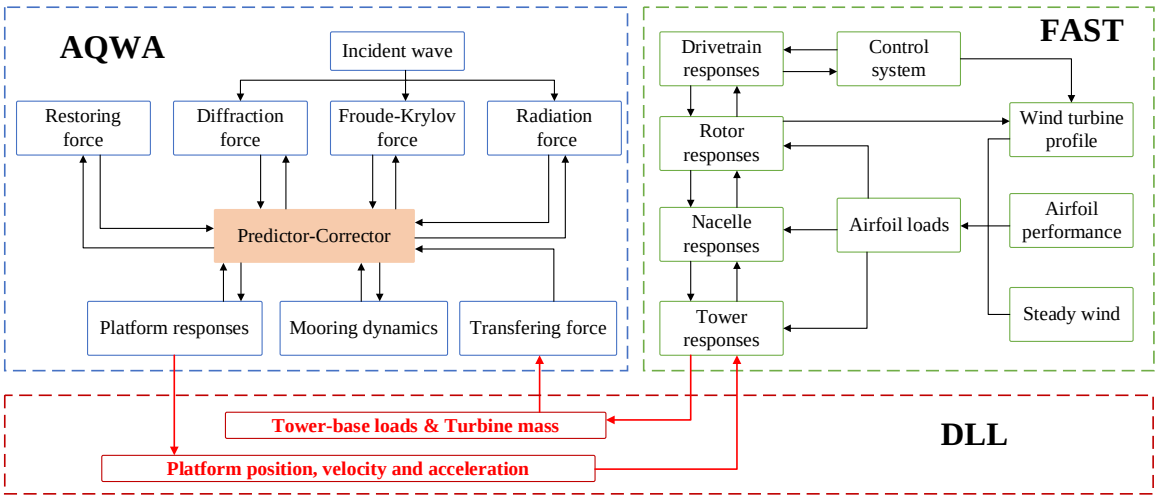

Figure 4 FAST-to-AQWA framework

3.4 Validation

In this section, the modelling of Wave Star in AQWA and the coupling function of F2A are validated.

3.4.1 Wave Star

The modelling of Wave Star in AQWA is validated against the experimental results proposed by Windt *et al*. [57]. The configuration of the 1:5 test model is shown in Figure 5 and Table 3. The wave period and height are T=1.4 s and H=0.1 m, respectively. Comparative results of the displacement of the hydraulic cylinder and the velocity of the piston are shown in Figure 6. A good agreement is achieved with a maximum difference of 4%.

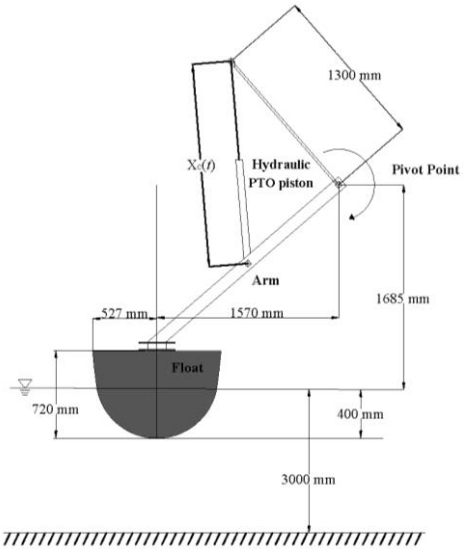

Figure 5 Sketch of Wave Star in ref. [57]

Table 3 Properties of the 1:5 Wave Star model

Item	Value and unit
Mass (Float & Arm)	220 kg
Inertia about the pivot point	1242 kg·m^2
X (CM relative to the hinge position)	1.3954 m
Y (CM relative to the hinge position)	0.0 m
Z (CM relative to the hinge position)	−1.3305 m
Submergence (in average position)	0.4 m
Water depth	3 m

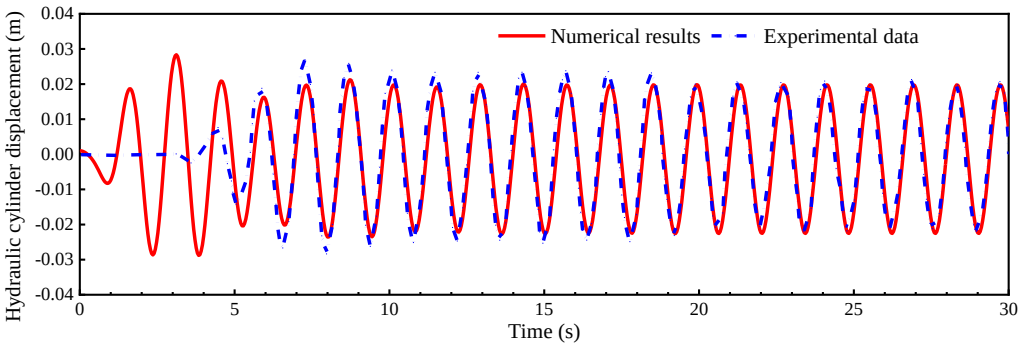

(a) Displacement of hydraulic cylinder

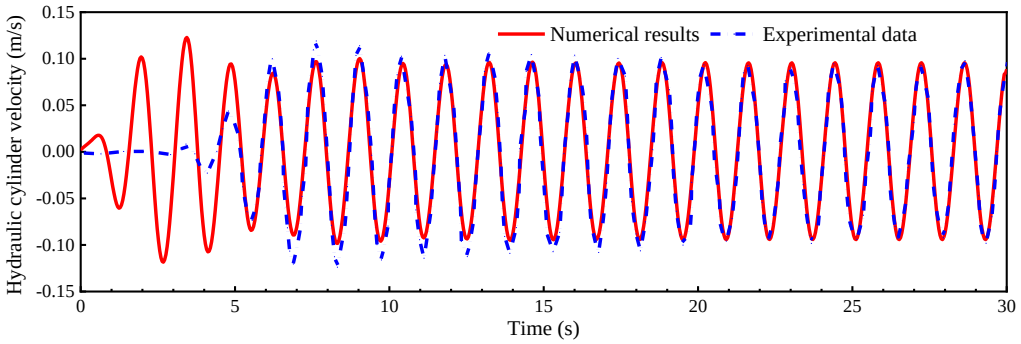

(b) Velocity of hydraulic piston

Figure 6 Comparisons of displacement of the hydraulic cylinder and velocity of the piston (b_{PTO}=0, T=1.4 *s*, H=0.1 m)

3.4.2 F2A

The coupling framework of F2A is validated against the HydroDyn module in FAST through a simulation of the DeepCWind platform. The configurations of the platform and mooring are shown in Table 1. The wave is normally incident, and the wave height is H=2 m. The wave period is T=4.5 s, 4.9 s, 5.3 s, 5.7 s, and 6.1 s. The wind speed is U=11.4 m/s. Comparative results of the surge, heave, and pitch motions, rotor speed, and the maximum mooring tensions of the three cables are shown in Figure 7. The results calculated by F2A and by HydroDyn match well in most cases. This indicates that the wind module of OpenFAST works well with AQWA in the present F2A framework, and AQWA can accomplish the hydrodynamic work of HydroDyn in OpenFAST. A large deviation in the pitch motion of the platform exists due to the use of different centres of rotation in F2A and HydroDyn [42], but it does not affect the use of AQWA in the F2A framework to calculate the relative motion between the platform and the Wave Star and the absorbed wave energy.

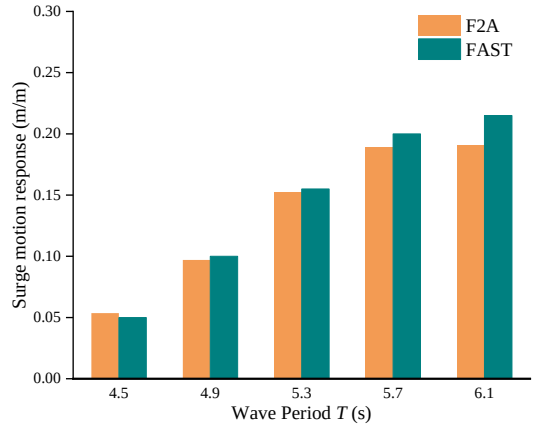

(a) Surge

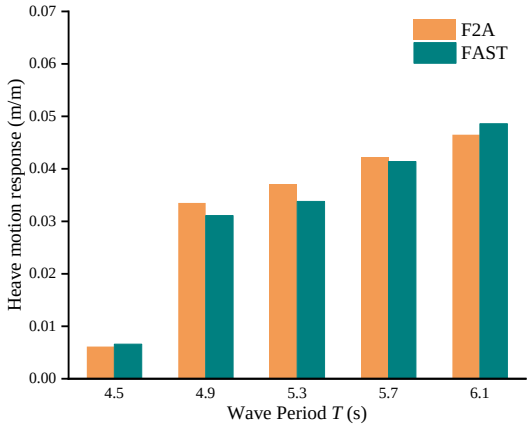

(b) Heave

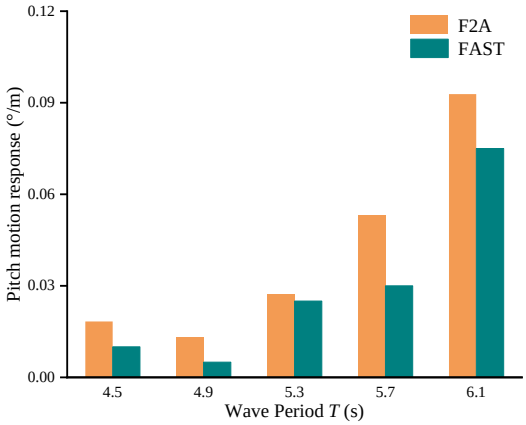

(c) Pitch

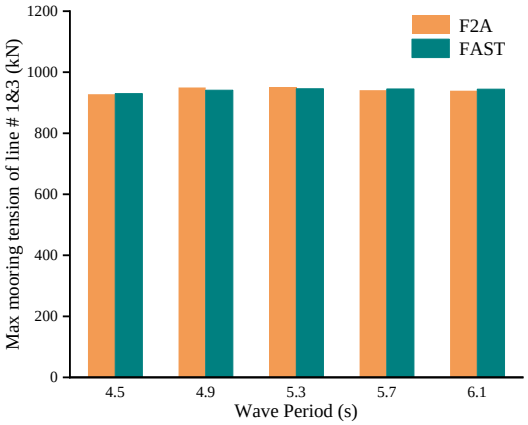

(d) Maximum mooring tension of line #1 & #3

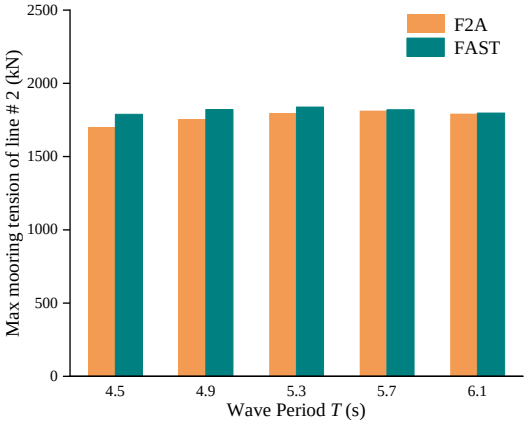

(e) Maximum mooring tension of line #2

Figure 7 Comparison of the dynamic response results calculated by AQWA and FAST

4. Numerical results and discussions

The wave power generation of the Wave Stars is optimized by applying an identical optimal PTO damping b_{opt} on all the devices, where it is obtained by numerical search [56]. The optimal PTO damping b_{opt} of a Wave Star with an arm projection L_h=22.87 m and a contained angle φ=30° in incident waves

from 4 s to 9 s and wind speed U=0, 8 m/s, 11.4 m/s, and 14 m/s are shown in Figure 8. Note that b_{opt} is much more sensitive to the change of wave period than the change of wind speed.

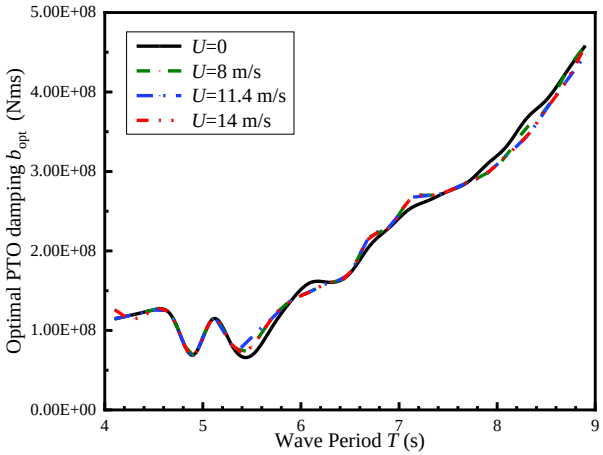

Figure 8 Optimal PTO damping under different wind and wave conditions

In all the following simulations, regular incident linear waves with a unit amplitude propagate in the positive x-direction. The water depth is 200 m. Steady uniform winds flow in the positive x-direction with speeds of 8 m/s, 11.4 m/s, and 14 m/s are employed.

4.1 Layout of Wave Stars

The influence of the layout of the Wave Stars on wave power generation is investigated. As shown in Eq. (1) and Figure 2, the layout of the Wave Stars is defined by the arm projection L_h (the distance from the central line of a Wave Star to the side column where it is installed) and the contained angle φ. A method is proposed to quickly define the two key parameters based on the distribution of wave amplitude (wave amplitude contour) in the surrounding region.

The wave amplitude contour in the region around a single DeepCWind platform is shown in Figure 9a. Due to the superposition of the incident wave and the radiated and diffracted waves generated by the platform, a band-like wave contour is formed (high waves with amplitude greater than incident waves in some stripped regions). Deploying Wave Stars right in the focusing regions can improve wave power generation, which is the optimization strategy to be used. The wave amplitude contour around a DeepCWind-Wave Stars hybrid system is shown in Figure 9c. In this case, the arm projection is L_h=22.87 m, and the contained angle is φ = 0. By integrating the WECs, the wave amplitude contour has negligible change compared with that around a single platform. Together with Figure 9b and d, it indicates that the wave amplitude contour is predominantly defined by the platform, and the optimization of the layout of Wave Stars by changing their positions will not significantly affect the wave contour. Then the wave contour can be used as a stable reference for optimizing the layout of Wave Stars.

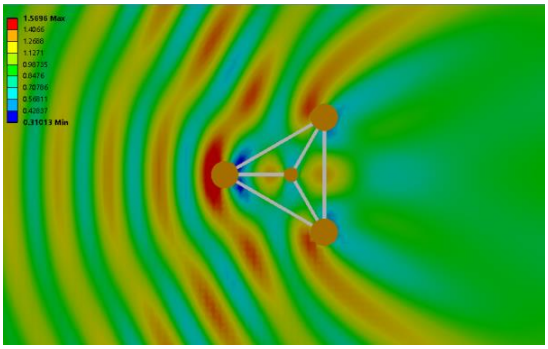

(a) Single Platform

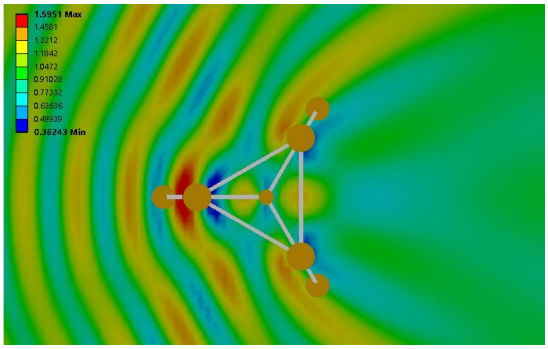

(b) Hybrid system (L_h=8.87 m)

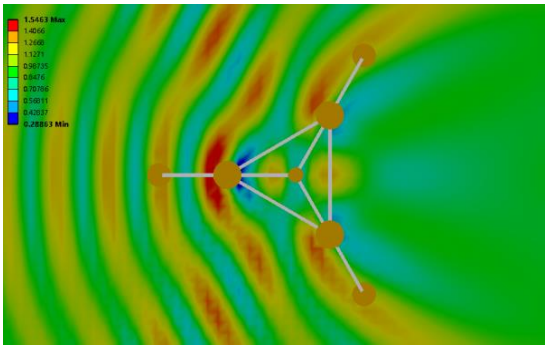

(c) Hybrid system (L_h=22.87 m)

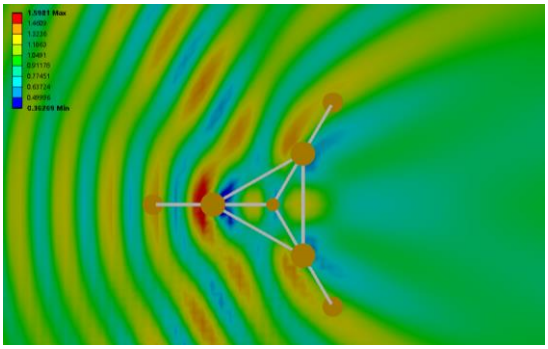

(d) Hybrid system (L_h=28.87 m)

Figure 9 Wave amplitude contour around single platform and hybrid system under T_p=5.3 s

The influence of the arm projection L_h on wave power generation is first investigated. The tendency of wave power and wave amplitude along the direction of the arm are also compared. The contained angle is set as φ=0. Figure 10 shows the wave power and amplitude for a range of arm projection lengths under the incident wave of T_p=5.3 s. Figure 10a shows that the tendency of the wave power of WEC #2 is similar to that of the wave amplitude but with a slight drift to larger L_h. This deviation is caused by the addition of the WEC has a small disturbance on the local wave amplitude by diffraction and radiation. Figure 10b shows that while the distance between WEC #1 or WEC #3 and the corresponding side column is far, the tendency of wave power is coherent with that of the wave amplitude. The radiation and diffraction of the WEC also cause a little deviation. Both Figure 10a and Figure 10b show that while a WEC is close to the side column, its power generation dramatically increases. This is due to the complex radiation and diffraction as the device is placed close to the column [58]. In this mode, water resonates in the narrow gap between the Wave Star and the side column, inducing a very high wave force that promotes the motion of the Wave Star to obtain a large power output. Figure 10c shows the tendency of the total power generation, which is similar to that of WEC #2. The maximum wave power can be obtained at L_h=25.13 m, while the maximum wave amplitude occurs at L_h=22.87 m. Although the maximum power cannot be obtained when the Wave Stars are precisely placed where the highest wave amplitude exists due to the disturbance of the platform, the difference (2.26 m) is not significant

compared with the radius of the Wave Star, and the power output only decreases by 7.06%. Therefore, for rapid design of the layout of the Wave Stars, the location of the highest wave amplitude can be used as a criterion. L_h=22.87 m is thereafter used as the optimal arm projection.

The optimal contained angle φ is then determined. Figure 11 shows the total wave power under contained angles φ = 0, 15°, 22°, 30°, 37°, and 45° while the arm projection remains L_h=22.87 m. The total power first increases and then decreases as the contained angle grows, peaking at φ=30°. From the perspective of power output maximization, the arm projection L_h=22.87 m and included angles φ=30° are regarded as the optimized layout of the Wave Stars, which will be used in the rest of the analysis.

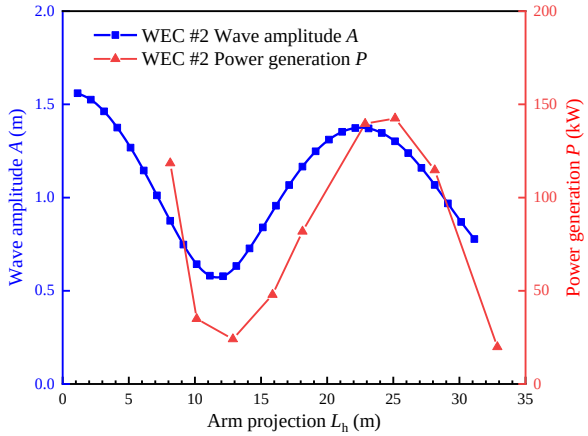

(a) WEC #2

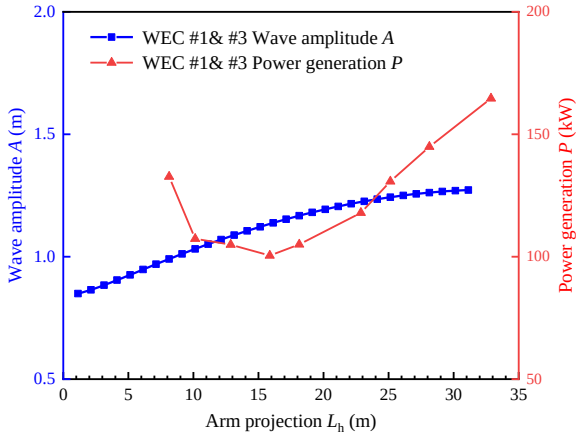

(b) WEC #1 or #3

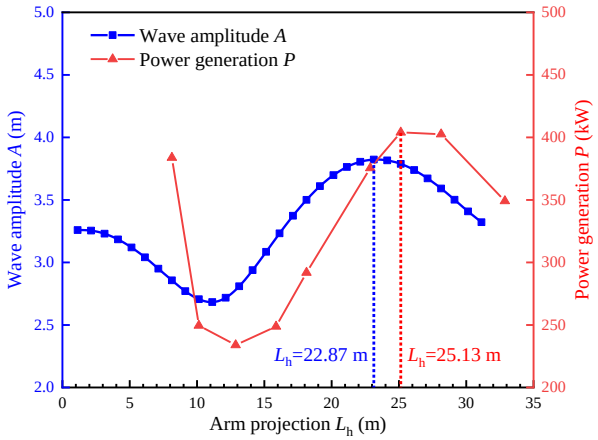

(c) Total power

Figure 10 The power generation and amplitude for different arm projections (T=5.3 s, φ=0°)

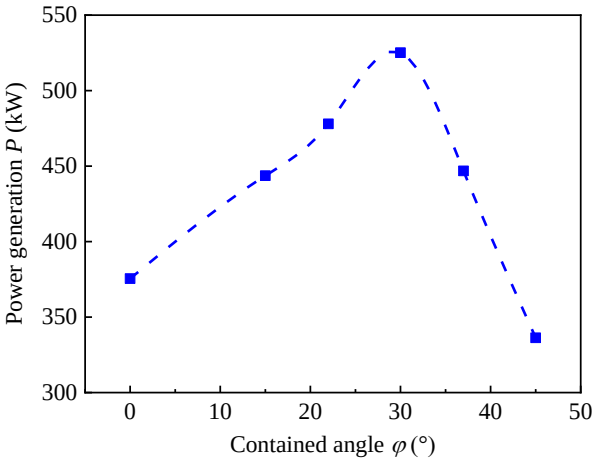

Figure 11 The power generation for different included angles (T=5.3 s, L_h=22.87 m)

4.2 Motion of the platform

The influence of the Wave Stars on the motions, including the equilibrium position and the response amplitudes of the DeepCWind platform, is analyzed. The arm projection of Wave Star is L_h=22.87 m, and the contained angle is φ=30°. The wind force is also considered by applying four wind speeds U=0, 8 m/s, 11.4 m/s, and 14 m/s, where U=11.4 m/s is the critical wind speed.

Figure 12 shows the equilibrium positions of the platform in surge, heave and pitch under different wind speeds and wave periods with and without the integration of Wave Stars. The regular incident wave is from T=4 s to 9 s with an increment of 0.1 s. Figure 12a shows that by integrating the Wave Stars, the equilibrium position of the platform in surge always increases under any wind and wave condition. This is because the diffraction force on the Wave Stars increases the total surge force on the hybrid system, driving the platform to drift farther than the equilibrium position of a single platform. Figure 12b shows that by integrating the Wave Stars, the equilibrium position of the platform in heave continuously decreases under any wind and wave condition. This is due to the presence of the Wave Stars adding the total buoyance of the system, which elevates the platform. Figure 12c shows that by integrating the Wave Stars. At the same time, there is no wind, and the position (angle) of equilibrium of the platform in pitch continuously decreases slightly because the Wave Stars increase the total hydrostatic restoration stiffness, making the hybrid system more resistant to the wind force in pitch. As wind presents, the angle of equilibrium of the platform in pitch always slightly increases in the vicinity of T_p=5.3 s and has little change otherwise. This is because the horizontal wave force produces an additional pitch moment, and in the vicinity of T_p=5.3 s, this effect is much more significant than at other periods. Although the hydrostatic restoration stiffness also increases, the additional wave torque causes a small increment of the angle of equilibrium.

For either surge, heave, or pitch, the equilibrium position of the platform first increases and then decreases as wind speed increases. A peak occurs for the critical wind speed U=11.4 m/s. This is coherent

with the trend of thrust force on the rotor against wind speed. In surge, the equilibrium position of the platform is determined by the horizontal component of the thrust force; in heave, the equilibrium position of the platform is determined by the balancing between the vertical component of the thrust force and buoyancy; in pitch, the angle of equilibrium of the platform is determined mainly by the balance between the torque generated by the horizontal thrust force and the hydrostatic restoration force.

A comparison between Figure 12a, b, and c reveals that in either the single platform or the hybrid system, wind speed influences the equilibrium positions of the platform much larger in surge and pitch than in heave. And compared with wave period, wind speed has a much larger influence on the equilibrium positions of the platform, which is a major factor in the design and evaluation of the motion of the platform. For example, in Figure 12a, the variation of the equilibrium position in surge can reach 8 m, whereas, in Figure 12b, the largest variation of the equilibrium position in heave is no larger than 0.1 m. Nevertheless, comparing the data in Figure 12a, b, or c, one can also find that the wind speed has almost little influence on the increment of the equilibrium position in either surge, heave, or pitch caused by the integration of the Wave Stars. Wave period influences such increments in the vicinity of the peak wave period T_p=5.3 s (where the Wave Stars resonate) but not large. These indicate that in designing and evaluating the hybrid system, once the configuration of the wind turbine is determined, the investigation of the influence of the wind condition on the motion of the hybrid system is not necessary. In contrast, wave period can be a factor to be considered but is unimportant. Finally, since the equilibrium position in pitch, which is a key factor that influences the stability of the system, is not affected, integrating the Wave Stars does little harm to the static stability of the original platform.

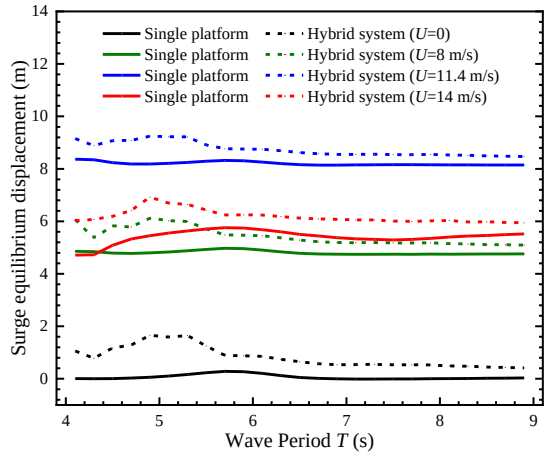

(a) Surge

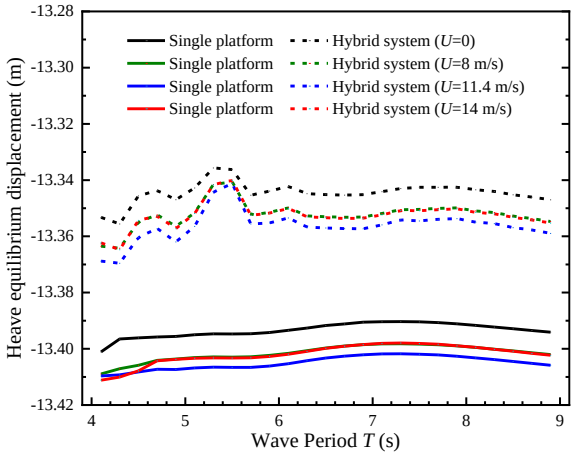

(b) Heave

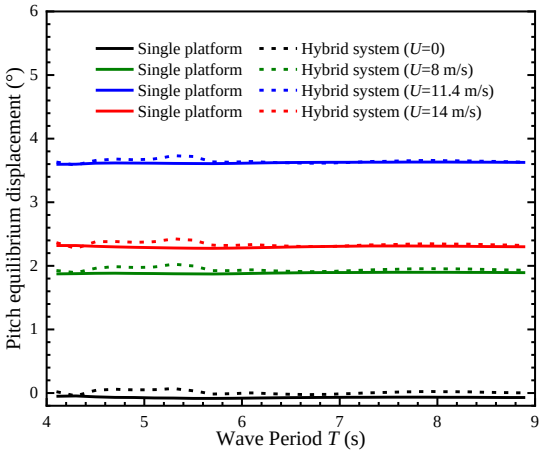

(c) Pitch

Figure 12 The equilibrium position of the platform under different wind and wave conditions

Figure 13 shows the surge, heave and pitch motions under different wind speeds and wave periods of the single platform and the hybrid system. The incident wave is from 4 s to 9 s with an increment of 0.5 s. The data under T_p = 5.3 s are individually given.

Figure 13a shows that the influence of the Wave Stars on the surge motion of the platform depends on the wind and wave condition, i.e., for different wind speeds and wave periods, the influence is different. In the vicinity of the peak wave period T_p = 5.3 s, the Wave Stars can reduce the surge motion of the platform by at most 45.19%, which enhances the stability of the platform in this condition. Figure 13b shows that similar to the surge motion, the influence of the Wave Stars on the heave motion of the platform also depends on the wind and wave conditions. In the vicinity of the peak wave period T_p = 5.3 s, the Wave Stars slightly reduce the heave motion of the platform by at most 24.84%, which slightly enhances the stability of the platform. Figure 13c shows that different from those in surge and heave, the influence of the Wave Stars on the pitch motion of the platform is independent of the wind and wave condition in most cases (except for T = 4 s). The Wave Stars can almost always increase the pitch motion of the platform. The reason is as follows. On the one hand, adding the Wave Stars increases the wave force; on the other hand, it also increases the hydrostatic restoration stiffness and damping in pitch. The increase in the wave force exceeds the increase in the hydrostatic restoration stiffness and damping, and the combined effect leads to a larger pitch motion.

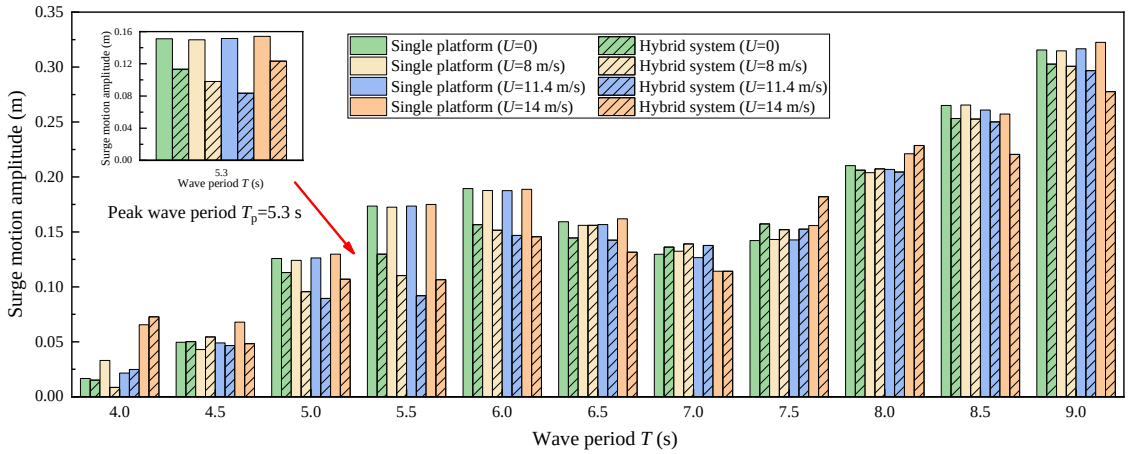

(a) Surge

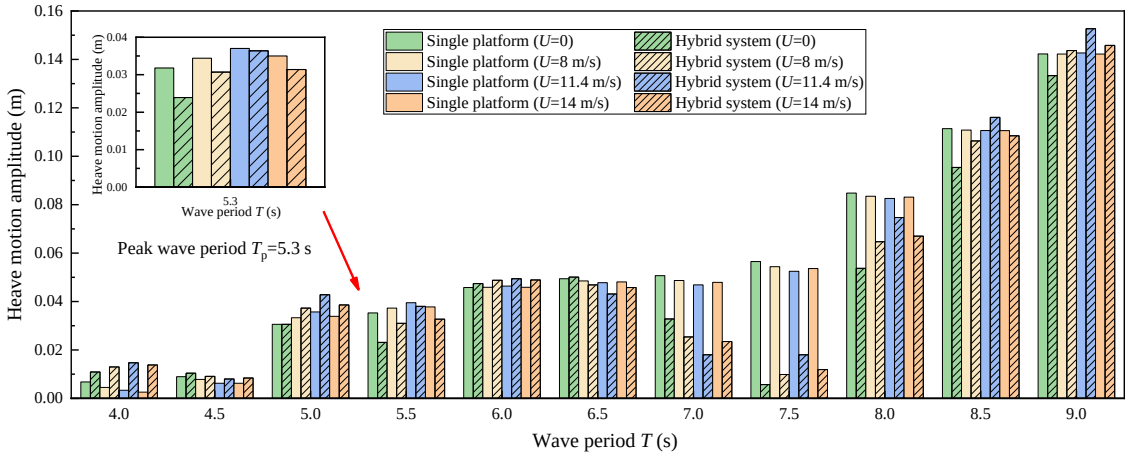

(b) Heave

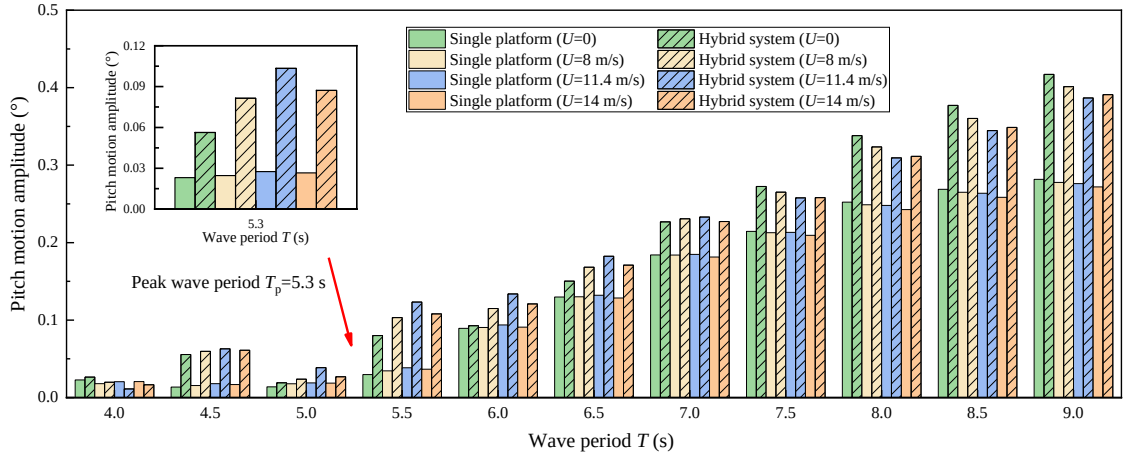

(c) Pitch

Figure 13 Platform motion for different wind speed

From Figure 13, the influence of wave conditions on the motions of either the single platform or the hybrid system is generally larger than the influence of wind conditions. This can be evident from the maximum difference between the motions under different wave periods and between the motions under different wind speeds. Take the pitch motions of the hybrid system as an example. For wind speed U=11.4 m/s, the difference between the pitch motions of T = 4 s and T = 9 s is 0.38°. For wave period T

= 9 s, the difference between the pitch motions of U=0 and U=11.4 m/s is only 0.03°. Besides, for any wave condition, the change of either surge, heave, or pitch motion of the hybrid system under different wind speeds is slightly larger than the change of the surge, heave, or pitch motion of the single platform, indicating that the motion of the hybrid system is slightly more sensitive to the wind condition than that of the single platform. However, the difference can be neglected. The motions of the single platform or the hybrid system are small in all wind and wave conditions. Considering the pitch motions, the Wave Stars only increase it by at most 0.13°, which is relatively small than the equilibrium position in pitch (2°~4° if in wind). Therefore, the Wave Stars nearly do not affect the dynamic stability of the platform.

4.3 Mooring tension

The influence of the Wave Stars on the mooring force exerted on mooring cable #2 (which bears the highest mooring load among the three) is evaluated. The regular incident wave period is from T = 4 s to T = 9 s with an increment of 0.1 s.

Figure 14a~d show the mean value (the large point) and amplitude (the segment stemmed from the large point) of the mooring force under wind speed U=0, 8 m/s, 11.4 m/s, and 14 m/s, respectively. Compared to Figure 12a, the tendency of the average mooring force of either the single platform or the hybrid system is quite similar to that of the equilibrium position in surge, indicating that the average mooring force is closely related to the surge motion of the platform. One can find that under any wind and wave conditions, the average mooring force always increases due to the integration of the Wave Stars, although the maximum difference is no more significant than 9.07% (U= 11.4 m/s, T = 5.5 s). This increase in the average mooring force originates from the additional wave diffraction force and buoyancy generated by the Wave Stars. Besides, for any wind condition, the mooring force amplitude decreases due to the integration of the Wave Stars in most wave conditions. The detailed results of the difference in the mooring force amplitude between the single platform and the hybrid system are also shown in Figure 15. Note that by integrating the Wave Stars, the maximum mooring tension is reduced near the peak wave period T_p = 5.3 s. The maximum reduction of mooring force amplitude occurs for T = 5.5 s. The fluctuation of mooring force is an essential indicator in predicting fatigue damage and the operational lifespan of mooring cables. A smaller fluctuation represents a lighter abrasion of mooring cables. From this viewpoint, integrating the Wave Stars on the platform can reduce the fatigue damage of the mooring cables, which improves the reliability of the mooring system.

A comparison between Figure 14a~d shows that as the wind speed increases, the average mooring force first increases and then decreases, reaching a maximum value at the critical wind speed U=11.4 m/s. The mooring force amplitude has no evident regular changing tendency along the wind speed. One can also find that under any wind condition, as the wave period increases, the average mooring force does not change much, whereas the mooring force amplitude changes relatively dramatically. The above

results reveal that the wind condition dominates the average mooring force. In contrast, the wave condition has a minor influence, which dominates the mooring force amplitude, whereas the wind condition has a limited impact. This indicates that wind speed should be a primary concern when designing the survivability threshold of the mooring cables of either a single platform or a hybrid system under extreme conditions. And in assessing the fatigue life of the mooring cables, wave condition should be a significant concern. An interesting phenomenon is that at T = 5.5 s, the mooring force amplitude of the single platform reaches a maximum local value, whereas that of the hybrid system reaches a local minimum value (which can also be revealed in Figure 15). This is because by adding the Wave Stars, the large mooring force amplitude caused by the resonance of the platform is primarily suppressed by the additional mass and damping induced by the Wave Stars.

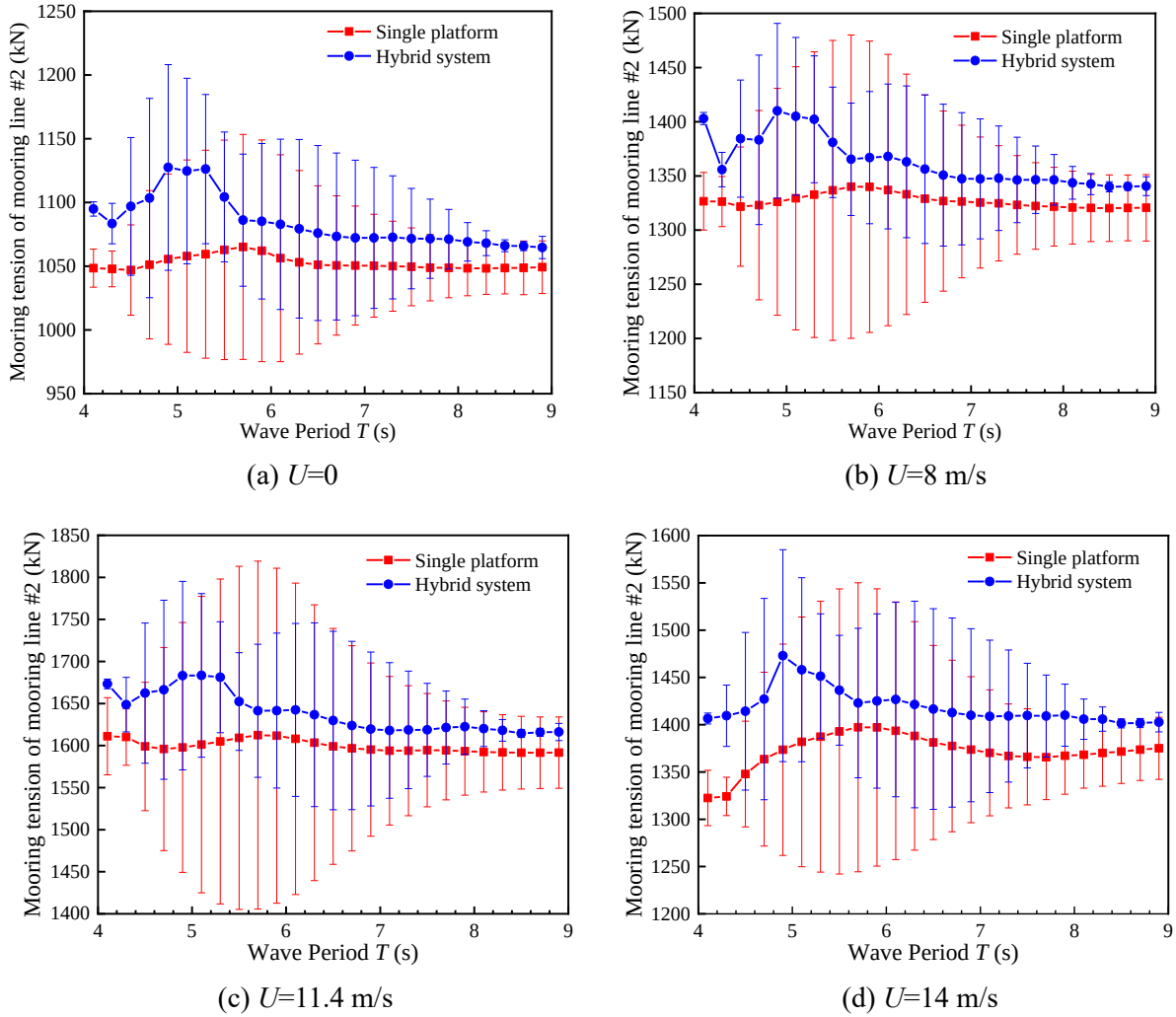

(a) U=0 (b) U=8 m/s

(c) U=11.4 m/s (d) U=14 m/s

Figure 14 Mooring tension of line #2 under different wind and wave conditions

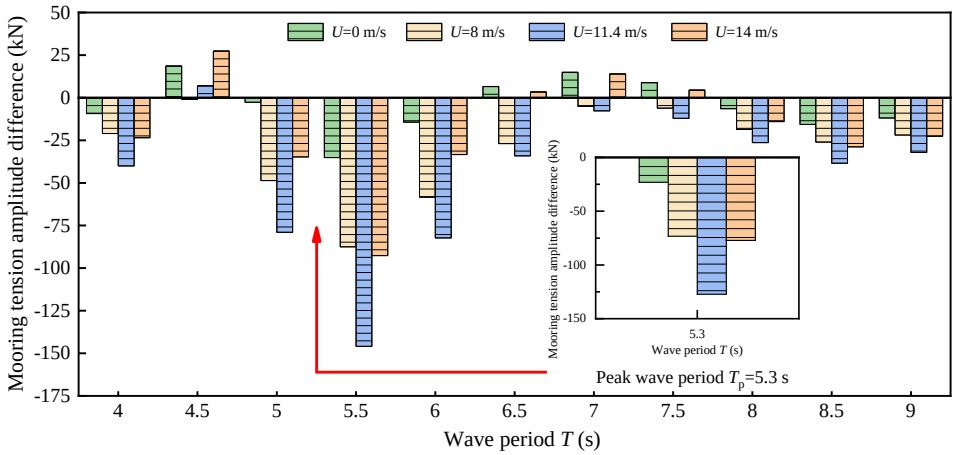

Figure 15 Difference in mooring tension amplitude between the single platform and the hybrid system

4.4 Power performance

In this section, the power performance of the hybrid system is evaluated and compared with that of a single wind turbine under a range of wind and wave conditions. Figure 16 shows the wave power generated by the Wave Stars. The regular incident wave is from T = 4 s to 9 s with an increment of 0.1 s. The wind speed is U=0, 8 m/s, 11.4 m/s, and 14 m/s. Comparing Figure 16a and Figure 16b, the influence of wind speed on the power generation of WEC #2 is much larger than and, in a way, quite different from that of WEC #1 or WEC #3. For WEC #2, compared with the condition of no wind, as wind presents, the power generation of WEC #2 increases at some wave periods and decreases at some others. Overall, the fluctuation in the power generation of WEC #2 is larger as wind is presented. The largest fluctuation occurs for the critical wind speed U=11.4 m/s, wherein the equilibrium positions of the platform have the largest changes. For WEC #1 or WEC #3, as wind presents, the power output slightly increases for every wave condition, and the difference in the power generation under different wind speeds is quite small. This phenomenon can be explained by how wind speed influences the equilibrium position of the platform in pitch. To WEC #2, as it is deployed directly along the x-direction, the change of the equilibrium position in pitch of the platform has a full influence on its contained angle. Whereas to WEC #1 or WEC #3, as they are oblique to the x-direction, the change of the equilibrium position in the pitch direction of the platform only partially influences their contained angle. Therefore, the influence of wind speed on WEC #2 is much larger than that of WEC #1 or WEC #3. From Figure 16c, in most cases, the wind has a slight promotion on the wave power absorption. The wave power generation in the hybrid system is quite stable in different wind conditions. Compared with wind, the wave has a much larger influence on the power generation of the Wave Stars, revealed by the sharp fluctuations. These fluctuations are primarily caused by the change in local wave height due to the diffraction and radiation of the platform in different waves. The power generation of the WECs remains nearly constant in long waves due to weak wave diffraction.

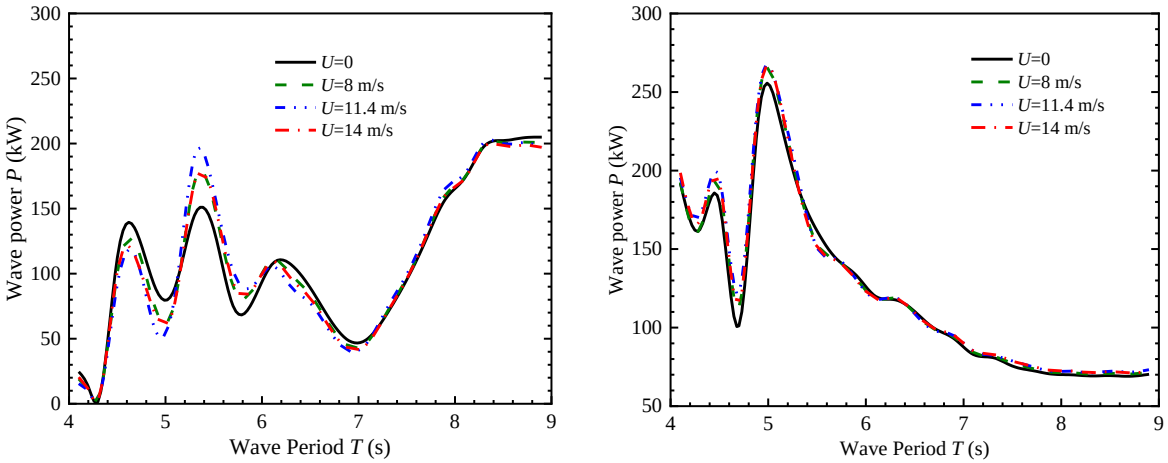

(a) WEC #2

(b) WEC #1 or #3

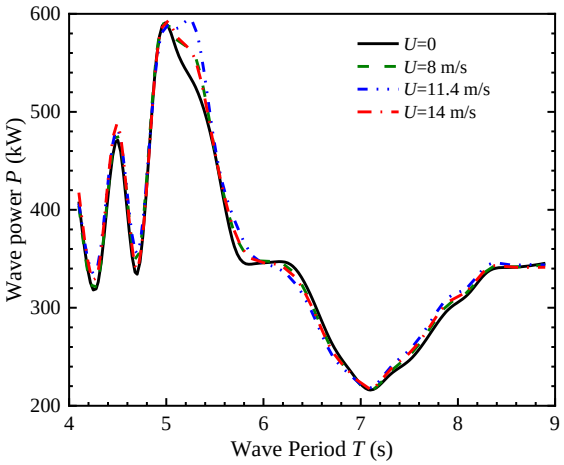

(c) Total power

Figure 16 Wave power generation under different wind and wave conditions

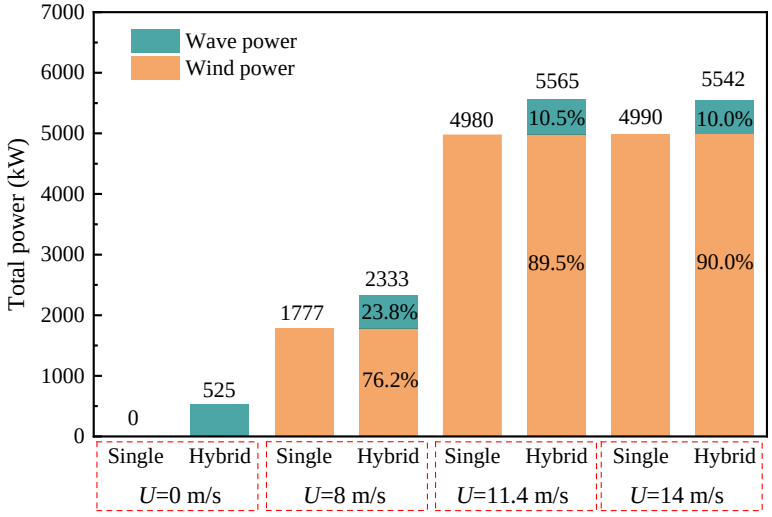

Figure 17 Power generation of the hybrid system at different wind speeds (T_p=5.3 s)

Figure 17 shows the total power generation (sum of wind and wave power) of the hybrid system and

the proportions of wind power and wave power. The regular incident wave is T_p=5.3 s. The wind speed is U=0, 8 m/s, 11.4 m/s, and 14 m/s. Under each wind condition, the Wave Stars can provide power over 500 kW, which can be valuable to the whole while the wind turbine is experiencing downtime. Besides, the integration of the Wave Stars does not reduce wind power. As wind speed increases, the proportion of wave power becomes smaller. As the wind speed reaches the critical speed of U=11.4 m/s, the proportion of the wave power keeps about 10%. Considering that in most situations, the average wind speed in the South China Sea is smaller than 10.7 m/s and the average wave height is larger than 2 m [14], the percentage of wave power in the total power generation can be larger than that in the U= 8 m/s (23.8%), which could be an effective supplement.

5. Conclusion

A novel DeepCWind-Wave Stars wind-wave hybrid system is proposed and the layout of the Wave Stars is optimized. The aero-hydro-servo couplings of the hybrid system are simulated by a combined toolkit of FAST, AQWA, and an F2A code. The influence of the Wave Stars on the platform's motions and mooring loads is investigated, and the power performance of the hybrid system is evaluated under a wide range of wind and wave conditions. The main findings are:

1. The optimal arm projection length and contained angle of the Wave Star can be quickly determined based on the wave amplitude contour in the region around the platform. This method can readily be used to design similar hybrid systems. Notably, the optimal arm projection length in the present hybrid system is 22.87 m, and the optimal contained angle is 30°.

2. The Wave Stars have the most considerable influence on the equilibrium position of the platform in the surge direction. In contrast, it has a trifling effect on the equilibrium positions of the platform in heave and pitch. The Wave Stars increase the pitch motion of the platform, but the overall influence is so small that it will not affect the stability of the platform.

3. The Wave Stars slightly increase the average mooring force, raising the survivability threshold of the mooring system. The Wave Stars also reduce the mooring force amplitude, reducing the fatigue damage on the mooring cables and improving the reliability of the mooring system.

4. The Wave Stars provide considerable power to the original DeepCWind floating offshore wind turbine, which is an essential supplement to the wind power and a robust regulation to the power output fluctuation while the turbine is experiencing downtime.

The limitations of this study are: 1) The investigation is based on numerical simulation in regular waves and steady winds. It does not consider all physical phenomena, such as irregular waves, extreme sea conditions, or turbulent wind, that may occur in real-world wind-wave hybrid systems. 2) The analysis is based on a specific hybrid system determined according to specific wave conditions at a

selected operation site. The results may not be generalizable to other hybrid systems or operating conditions. 3) The energy production efficiency loss in the transmission line and PTO are not considered.

Acknowledgement

This work is supported by the National Natural Science Foundation of China (52071096, 52201322, and 52222109), Guangdong Basic and Applied Basic Research Foundation (2022B1515020036), Fundamental Research Funds for the Central Universities (2022ZYGXZR014), and the Science Foundation of Donghai Laboratory (DH-2022KF0315). P. J. gratefully acknowledge the State Key Laboratory of Coastal and Offshore Engineering for supporting this work through the Open Research Fund Program (grant no. LP2214).

Reference

[1] Qiu, S., Liu, K., Wang, D., Ye, J., & Liang, F. (2019). A comprehensive review of ocean wave energy research and development in China. *Renewable and Sustainable Energy Reviews*, 113, 109271.

[2] Hu, H., Xue, W., Jiang, P., & Li, Y. (2022). Bibliometric analysis for ocean renewable energy: An comprehensive review for hotspots, frontiers, and emerging trends. *Renewable and Sustainable Energy Reviews*, 167, 112739.

[3] Quirapas, M. A. J. R., & Taeihagh, A. (2021). Ocean renewable energy development in Southeast Asia: Opportunities, risks and unintended consequences. *Renewable and Sustainable Energy Reviews*, 137, 110403.

[4] Pérez-Collazo, C., Greaves, D., & Iglesias, G. (2015). A review of combined wave and offshore wind energy. *Renewable and Sustainable Energy Reviews*, 42, 141-153.

[5] Astariz, S., & Iglesias, G. (2016). Co-located wind and wave energy farms: Uniformly distributed arrays. *Energy*, 113, 497-508.

[6] Gaughan, E., & Fitzgerald, B. (2020). An assessment of the potential for Co-located offshore wind and wave farms in Ireland. *Energy*, 200, 117526.

[7] Ren, Z., Verma, A. S., Li, Y., Teuwen, J. J., & Jiang, Z. (2021). Offshore wind turbine operations and maintenance: A state-of-the-art review. *Renewable and Sustainable Energy Reviews*, 144, 110886.

[8] Zhou, B., Zhang, Q., Jin, P., Li, Y., Liu, Y., Zheng, S., & Ning, D. (2022). Geometric asymmetry in the energy conversion and wave attenuation of a power-take-off-integrated floating breakwater. *Ocean Engineering*, 246, 110576.

[9] Qiao, D., Haider, R., Yan, J., Ning, D., & Li, B. (2020). Review of wave energy converter and design of mooring system. *Sustainability*, 12(19), 8251.

[10] Zhang, H., Zhou, B., Vogel, C., Willden, R., Zang, J., & Zhang, L. (2020). Hydrodynamic

performance of a floating breakwater as an oscillating-buoy type wave energy converter. *Applied Energy*, 257, 113996.

[11] Chen, X., Wang, K., Zhang, Z., Zeng, Y., Zhang, Y., & O'Driscoll, K. (2017). An assessment of wind and wave climate as potential sources of renewable energy in the nearshore Shenzhen coastal zone of the South China Sea. *Energy*, 134, 789-801.

[12] Clemente, D., Rosa-Santos, P., & Taveira-Pinto, F. (2021). On the potential synergies and applications of wave energy converters: A review. *Renewable and Sustainable Energy Reviews*, 135, 110162.

[13] Astariz, S., & Iglesias, G. (2015). The economics of wave energy: A review. *Renewable and Sustainable Energy Reviews*, 45, 397-408.

[14] Hu, J., Zhou, B., Vogel, C., Liu, P., Willden, R., Sun, K., ... & Collu, M. (2020). Optimal design and performance analysis of a hybrid system combing a floating wind platform and wave energy converters. *Applied Energy*, 269, 114998.

[15] Zhang, H., Zhou, B., Zang, J., Vogel, C., Fan, T., & Chen, C. (2021). Effects of narrow gap wave resonance on a dual-floater WEC-breakwater hybrid system. *Ocean Engineering*, 225, 108762.

[16] Zhang, H., Zhou, B., Zang, J., Vogel, C., Jin, P., & Ning, D. (2021). Optimization of a three-dimensional hybrid system combining a floating breakwater and a wave energy converter array. *Energy Conversion and Management*, 247, 114717.

[17] Chozas, J. F., Sørensen, H. C., & Jensen, N. H. (2012). Economic benefit of combining wave and wind power productions in day-ahead electricity markets. *In 4th International Conference on Ocean Energy*.

[18] Chozas, J. F., Kofoed, J. P., & Sørensen, H. C. (2013). Predictability and Variability of Wave and Wind: wave and wind forecasting and diversified energy systems in the Danish North Sea. Department of Civil Engineering, Aalborg University. DCE Technical reports No. 156.

[19] Zhou, Y., Ning, D., Chen, L., & Iglesias, G. (2021). Nonlinear hydrodynamic modeling of an offshore stationary multi-oscillating water column platform. *Ocean Engineering*, 227, 108919.

[20] Tian, W., Wang, Y., Shi, W., Michailides, C., Wan, L., & Chen, M. (2023). Numerical study of hydrodynamic responses for a combined concept of semisubmersible wind turbine and different layouts of a wave energy converter. *Ocean Engineering*, 272, 113824.

[21] Wan, L., Gao, Z., Moan, T., & Lugni, C. (2016). Experimental and numerical comparisons of hydrodynamic responses for a combined wind and wave energy converter concept under operational conditions. *Renewable Energy*, 93, 87-100.

[22] Ren, N., Ma, Z., Shan, B., Ning, D., & Ou, J. (2020). Experimental and numerical study of dynamic responses of a new combined TLP type floating wind turbine and a wave energy converter under operational conditions. *Renewable Energy*, 151, 966-974.

[23] Michailides, C., Gao, Z., & Moan, T. (2016). Experimental study of the functionality of a semi-submersible wind turbine combined with flap-type Wave Energy Converters. *Renewable Energy*, 93, 675-690.

[24] Platform, M. A. R. I. N. A. European Union Seventh Framework Programme (EU FP7) Marine Renewable Integrated Application Platform (MARINA Platform).

[25] Balat, M. (2009). A review of modern wind turbine technology. *Energy Sources*, Part A, 31(17), 1561-1572.

[26] Islam, M. R., Guo, Y., & Zhu, J. (2014). A review of offshore wind turbine nacelle: Technical challenges, and research and developmental trends. *Renewable and Sustainable Energy Reviews*, 33, 161-176.

[27] Saruwatari, M., Yun, K., Iwakuma, M., Tamura, K., Hase, Y., Sasamori, Y., & Izumi, T. (2016). Design study of 15-MW fully superconducting generators for offshore wind turbine. *IEEE Transactions on Applied Superconductivity*, 26(4), 1-5.

[28] Wu, X., Hu, Y., Li, Y., Yang, J., Duan, L., Wang, T., ... & Liao, S. (2019). Foundations of offshore wind turbines: A review. *Renewable and Sustainable Energy Reviews*, 104, 379-393.

[29] Shi, W., Zeng, X., Feng, X., Shao, Y., & Li, X. (2023). Numerical study of higher-harmonic wave loads and runup on monopiles with and without ice-breaking cones based on a phase-inversion method. *Ocean Engineering*, 267, 113221.

[30] Jiang, Z. (2021). Installation of offshore wind turbines: A technical review. *Renewable and Sustainable Energy Reviews*, 139, 110576.

[31] Nielsen K, Krogh J, Brodersen HJ, Steenstrup PR, Pilgaard H, Marquis L, Friis-Madsen E, Kofoed JP. Partnership for wave power-roadmaps. DCE Technical Report; 2015.

[32] Hansen, R. H., & Kramer, M. M. (2011). Modelling and control of the wavestar prototype. *In Proceedings of the 9th European Wave and Tidal Energy Conference*, EWTEC 2011. University of Southampton.

[33] Kamarlouei, M., Gaspar, J. F., Calvario, M., Hallak, T. S., Mendes, M. J., Thiebaut, F., & Soares, C. G. (2020). Experimental analysis of wave energy converters concentrically attached on a floating offshore platform. *Renewable Energy*, 152, 1171-1185.

[34] Gaspar, J. F., Kamarlouei, M., Thiebaut, F., & Soares, C. G. (2021). Compensation of a hybrid platform dynamics using wave energy converters in different sea state conditions. *Renewable Energy*, 177, 871-883.

[35] Si, Y., Chen, Z., Zeng, W., Sun, J., Zhang, D., Ma, X., & Qian, P. (2021). The influence of power-take-off control on the dynamic response and power output of combined semi-submersible floating wind turbine and point-absorber wave energy converters. *Ocean Engineering*, 227, 108835.

[36] Ghafari, H. R., Ghassemi, H., & He, G. (2021). Numerical study of the Wavestar wave energy

converter with multi-point-absorber around DeepCwind semi-submersible floating platform. *Ocean Engineering*, 232, 109177.

[37] Muliawan, M. J., Karimirad, M., & Moan, T. (2013). Dynamic response and power performance of a combined spar-type floating wind turbine and coaxial floating wave energy converter. *Renewable Energy*, 50, 47-57.

[38] Yde, A., Pedersen, M. M., Bellew, S. B., Køhler, A., Clausen, R. S., & Wedel Nielsen, A. (2014). Experimental and Theoretical Analysis of a Combined Floating Wave and Wind Energy Conversion Platform. DTU Wind Energy E No. 0044.

[39] Karimirad, M., & Koushan, K. (2016, November). WindWEC: Combining wind and wave energy inspired by hywind and wavestar. I*n 2016 IEEE International Conference on Renewable Energy Research and Applications* (ICRERA) (pp. 96-101). IEEE.

[40] Gao, Z., Moan, T., Wan, L., & Michailides, C. (2016). Comparative numerical and experimental study of two combined wind and wave energy concepts. *Journal of Ocean Engineering and Science*, 1(1), 36-51.

[41] Luan, C., Michailides, C., Gao, Z., & Moan, T. (2014, June). Modeling and analysis of a 5 MW semi-submersible wind turbine combined with three flap-type wave energy converters. In *International Conference on Offshore Mechanics and Arctic Engineering* (Vol. 45547, p. V09BT09A028). American Society of Mechanical Engineers.

[42] Yang, Y., Bashir, M., Michailides, C., Li, C., & Wang, J. (2020). Development and application of an aero-hydro-servo-elastic coupling framework for analysis of floating offshore wind turbines. Renewable Energy, 161, 606-625.

[43] Zhang, D., Chen, Z., Liu, X., Sun, J., Yu, H., Zeng, W., ... & Si, Y. (2022). A coupled numerical framework for hybrid floating offshore wind turbine and oscillating water column wave energy converters. *Energy Conversion and Management*, 267, 115933.

[44] Chen, M., Xiao, P., Zhou, H., Li, C. B., & Zhang, X. (2022). Fully coupled analysis of an integrated floating wind-wave power generation platform in operational sea-states. *Frontiers in Energy Research*, 10, 931057.

[45] Ransley, E. J., Greaves, D. M., Raby, A., Simmonds, D., Jakobsen, M. M., & Kramer, M. (2017). RANS-VOF modelling of the wavestar point absorber. *Renewable Energy*, 109, 49-65.

[46] Zeng, X., Shi, W., Feng, X., Shao, Y., & Li, X. (2023). Investigation of higher-harmonic wave loads and low-frequency resonance response of floating offshore wind turbine under extreme wave groups. *Marine Structures*, 89, 103401.

[47] Robertson A, Jonkman J, Masciola M, Song, H, Goupee, A, Coulling, A, Luan, C. *Definition of the semi-submersible floating system for phase II of OC4* [R]. National Renewable Energy Lab. (NREL), Golden, CO (United States), 2014.

[48] Zhang, L., Shi, W., Zeng, Y., Michailides, C., Zheng, S., & Li, Y. (2023). Experimental investigation on the hydrodynamic effects of heave plates used in floating offshore wind turbines. *Ocean Engineering*, 267, 113103.

[49] Jonkman, J. M., & Buhl, M. L. (2005). FAST user's guide (Vol. 365, p. 366). Golden, CO, USA: National Renewable Energy Laboratory.

[50] ANSYS, A. (2016). AQWA user's manual release 17.0. ANSYS Inc.: Canonsburg, PA, USA.

[51] Cummins, W. E., Iiuhl, W., & Uinm, A. (1962). The impulse response function and ship motions.

[52] Liu, Y. (2015). A Coupled Approach for Dynamic Modelling of a Semi-submersible Type Platform with Multiple Diffuser-Augmented Wind Turbines (Doctoral dissertation, Kyushu University).

[53] Shabana, A. A. (2020). Dynamics of multi-body systems. *Cambridge University Press*.

[54] Cao, H., Tang, Y. G., Tao, H. C., & Qin, Y. (2013). Design and frequency domain analysis of semi-submersible floating foundation for offshore wind turbine. *Ocean Engineering*, 31(2), 61-67.

[55] Zhou, B. Z., Hu, J. J., Sun, K., Liu, Y., & Collu, M. (2020). Motion response and energy conversion performance of a heaving point absorber wave energy converter. *Frontiers in Energy Research*, 8, 553295.

[56] Zhou, B., Hu, J., Jin, P., Sun, K., Li, Y., & Ning, D. (2023). Power performance and motion of a floating wind platform and multiple heaving wave energy converters hybrid system. *Energy*, 265, 126314.

[57] Windt C, Davidson J, Ransley E J, et al. Validation of a CFD-based numerical wave tank model for the power production assessment of the WaveStar ocean wave energy converter. *Renewable Energy*, 2020, 146: 2499-2516.

[58] Zhang, H., Zhou, B., Vogel, C., Willden, R., Zang, J., & Geng, J. (2020). Hydrodynamic performance of a dual-floater hybrid system combining a floating breakwater and an oscillating-buoy type wave energy converter. *Applied Energy*, 259, 114212.

[59] Liu, Y., Hu, C., Sueyoshi, M., Yoshida, S., Iwashita, H., & Kashiwagi, M. (2021). Motion response characteristics of a Kyushu-University semi-submersible Floating Wind Turbine with trussed slender structures: Experiment vs. numerical simulation. *Ocean Engineering*, 232, 109078.

[60] Jonkman, J. (2010). Definition of the Floating System for Phase IV of OC3 (No. NREL/TP-500-47535). National Renewable Energy Lab.(NREL), Golden, CO (United States).